Airflow Determines Natural Airborne Transmission of Tuberculosis in a Guinea Pig Model

Kubra F. Naqvi[1], Yuhui Guo[2], Deepak Sapkota[2], Pei Lu[1], Shibo Wang[2], Beatriz R. S. Dias[1], Victoria A. Ektnitphong[1], Arabella E. Martin[1], Bret M. Evers[3], Lenette L. Lu[1,4], Hui Ouyang[2*], Lydia Bourouiba[5*] and Michael U. Shiloh[1,6*]

[1] Department of Internal Medicine, University of Texas Southwestern Medical Center, Dallas, TX

[2] Department of Mechanical Engineering, University of Texas at Dallas, Richardson, TX

[3] Department of Pathology, University of Texas Southwestern Medical Center, Dallas, TX

[4] Department of Immunology, University of Texas Southwestern Medical Center, Dallas, TX

[5] The Fluid Dynamics of Disease Transmission Laboratory, Fluids and Health Network, Massachusetts Institute of Technology, Cambridge, MA

[6] Department of Microbiology, University of Texas Southwestern Medical Center, Dallas, TX

* Correspondence: Michael.shiloh@utsouthwestern.edu; lbouro@mit.edu; Hui.Ouyang@utdallas.edu

ABSTRACT

Tuberculosis (TB) spreads through the air when *Mycobacterium tuberculosis* (Mtb) passes from infected to susceptible hosts, yet the environmental, biophysical and microbial factors governing this process remain poorly understood. In the early twentieth century, Perla and Lurie used guinea pigs to demonstrate natural airborne transmission of Mtb, but such studies have not been revisited in the modern biosafety era. Here, we developed an aerodynamically-optimized guinea pig housing system that models natural, airborne, animal-to-animal Mtb transmission under biosafety level 3 (BSL-3) containment. Iterative engineering and particle transport experiments revealed that airflow is a critical determinant of transmission efficiency. Static housing and excessive unidirectional ventilation both eliminated transmission, whereas controlled, low-velocity airflow enabled aerosol particle retention and exposure of naïve animals. Under these optimized conditions, recipient guinea pigs converted their tuberculin skin tests above a defined positive threshold, developed Mtb-specific antibody responses, and exhibited pulmonary inflammation consistent with infection. These findings demonstrate that flow rates govern natural transmission of Mtb and provide a reproducible small-animal model for studying bacterial, host, and environmental factors that drive infectious spread. By reviving a century-old experimental paradigm with modern physics, engineering and immunologic tools, this work establishes a platform to dissect the mechanisms underlying airborne transmission of tuberculosis.

INTRODUCTION

Tuberculosis (TB), caused by *Mycobacterium tuberculosis* (Mtb) infection, remains one of the leading causes of infectious mortality worldwide (2024). Interrupting the

transmission cascade is essential to reducing global incidence, yet progress is hindered by an incomplete understanding of the host, bacterial and environmental factors that govern the spread of infection. Reliable animal models that recapitulate natural transmission are needed to dissect these factors and to accelerate development of transmission-blocking interventions and vaccines.

Guinea pigs have played a central role in the history of TB research (Donald et al., 2018). In 1882, Robert Koch established their use as a model for TB pathogenesis, noting that naïve animals housed near infected ones occasionally developed “spontaneous” pulmonary disease (Koch, 1882; Koch, 1912). In the 1920s and 1930s, David Perla and Max Lurie expanded on these observations, demonstrating that healthy guinea pigs co-housed with infected animals developed bronchogenic tuberculosis, and that transmission could occur even between animals housed in separate cages within the same room (Lurie, 1930a; Lurie, 1930b; Lurie, 1930c; Perla, 1927a; Perla, 1927b). These seminal studies provided the first experimental evidence for airborne transmission of Mtb. Decades later, Riley, Wells, and Mills extended this concept to humans, showing that air exhausted from TB wards could infect sentinel guinea pigs (Riley, 2001; Riley et al., 1962; Riley et al., 1957; Wells, 1955; Wells et al., 1948). Despite these pioneering efforts, little progress has been made over the past century toward developing a controlled small-animal system for experimental TB transmission.

Recent studies using minipigs (Ramos et al., 2017) and ferrets (Gupta et al., 2022) have demonstrated animal-to-animal transmission of Mtb, but these models require high infectious doses and lack correlation with natural respiratory behaviors such as coughing. The guinea pig remains an ideal species to model transmission: it is relatively

low-cost compared to other models, develops necrotizing granulomas similar to humans (Orme and Ordway, 2016), harbors Mtb within its airways during infection (Podell et al., 2014), and exhibits respiratory neurophysiology closely resembling that of humans (Canning, 2008; Mazzone et al., 2005). While guinea pigs have long been used as sentinels for human-to-animal transmission in air sampling studies (Dharmadhikari et al., 2011; Nardell, 1999; Riley et al., 1962; Riley et al., 1957; Stoltz et al., 2025), a modern system that supports natural guinea pig-to-guinea pig transmission via airborne particles under biosafety level 3 (BSL-3) conditions has not been established.

A key step in Mtb transmission is the generation and survival of aerosolized, pathogen-containing particles capable of reaching the alveoli of a new host. Respiratory maneuvers such as coughing (Fennelly et al., 2012; Fennelly et al., 2004; Loudon and Spohn, 1969; Tristao et al., 2025; Turner and Bothamley, 2015), sneezing (Duguid, 1946), singing (Loudon and Roberts, 1968; Mangura et al., 1998), and breathing (Dinkele et al., 2022) all produce aerosols containing Mtb. Once expelled, these particles are shaped by environmental factors such as desiccation, humidity, ventilation, and settling (Bourouiba, 2021) that determine their persistence and infectivity (Brown et al., 2025; Mishra et al., 2025; Singh et al., 2025). Modeling these processes in experimental systems is particularly challenging under BSL-3 conditions, where high ventilation rates designed for personnel safety can markedly reduce airborne particle retention.

Here, we describe the development of a guinea pig housing system engineered for natural Mtb transmission of Mtb. Through iterative transmission trials and particle transport measurements, we identify airflow as a critical determinant of transmission

efficiency. Transmission attempts using static housing and strong unidirectional airflow resulted in no detectable transmission, underscoring the critical role of cage design, ventilation rates, flow physics, and particle residence time in facilitating Mtb transmission. To address this, we modeled and tested the flow physics components of the designs under both ambient and BSL3 negative-pressure conditions. These experiments identified ventilation and cage design regimes that maximized aerosolized pathogen-laden microdroplet retention and distribution to the recipient side, thereby increasing the probability of successful host-to-host transmission. Using this refined system, we demonstrate that naïve guinea pigs co-housed with infected donors but separated by a permeable barrier mount Mtb-specific cellular and humoral immune responses and develop pulmonary inflammation. This work revives a classical model of airborne Mtb transmission with modern engineering precision, demonstrates that exposure or proximity alone are not sufficient to mediate airborne Mtb transmission, highlights the critical role of airflow and ventilation in transmission, and establishes a reproducible platform for dissecting the biophysical, environmental, microbial and host factors that drive the spread of Mtb.

RESULTS

Airflow is a critical driver of transmission

Because early transmission studies in guinea pigs were performed in cages with likely static airflow (Lurie, 1930b), we hypothesized that a similar approach could serve as a foundation for a modern experimental system. We therefore tested the first iteration of our guinea pig transmission system (system 0) by co-housing naïve recipient guinea pigs with Mtb-infected donors, separated by a perforated plexiglass barrier for 12

months (Fig. 1A, B). Infection of naïve animals was monitored bimonthly by tuberculin skin testing (TST).

This initial design emphasized simplicity, low-cost and ease of access to system components. We modified an existing static cage by inserting a plexiglass divider containing large holes to separate donor and recipient animals (Fig. 1B). The cages were housed on a metal shelving system located in the most negatively pressurized room of our ABSL3 facility (relative negative pressure -0.06 WC). Because guinea pigs are highly susceptible to progressive tuberculosis following low-dose infection (50-100 CFU) (Orme and Ordway, 2016), infected donors were replaced every 7-8 weeks to maintain a constant infectious source. After 12 months of exposure, none of the recipient animals converted their TSTs or showed clinical or histopathologic evidence of infection, and no Mtb CFU were recovered at necropsy.

The absence of transmission under these conditions contrasted sharply with historical reports from Perla and Lurie and suggested that modern biosafety engineering constraints might fundamentally alter airflow compared to the open systems used a century ago. In contemporary BSL-3 facilities, negative-pressure ventilation ensures containment but may also disrupt airborne particle movement between animals. We therefore reasoned that introducing controlled, unidirectional airflow from infected to naïve compartments could facilitate transport of infectious aerosols.

To test this, we modified a commercially available guinea pig housing system (Allentown, Inc.) to create “system 1” (Fig. 1C, D). The new design incorporated a stainless-steel barrier perforated with two panels of holes positioned at the typical nose and mouth height of an adult guinea pig. To establish unidirectional airflow, we blocked

the donor-side exhaust port (right) and the recipient-side supply ports (left) with rubber caps (Fig. 1E). Smoke testing confirmed right-to-left airflow from the donor to the recipient compartment (Fig. 1F, Suppl. Movie 1). Recipient animals were then exposed to infected donors for 12 months under these unidirectional airflow conditions. Despite these adjustments, no transmission occurred: all recipients remained TST-negative and free of histopathologic or microbiologic evidence of infection.

These findings demonstrated that simply imposing unidirectional airflow was insufficient to drive natural Mtb transmission. Instead, they highlighted the need for quantitative optimization of airflow rate and associated particle retention to enable sustained exposure of naïve animals to infectious aerosols generated by donor guinea pigs.

Airflow and cage design influence particle dynamics

The inability of systems 0 and 1 to support transmission suggested that airflow and cage architecture critically influence the movement and retention of airborne particles. We therefore undertook an iterative series of aerosol studies to define the parameters that would permit infectious particle transport from donor to recipient compartments.

To test aerosolized particle transport, we connected prototype cages to a supply air line on the donor side and an exhaust vacuum on the recipient side, allowing controlled regulation of airflow within the system. To simulate infectious particles, we used a particle generator to produce aerosols ranging from 0.8-7 µm and sampled air at three locations: upstream (before entering the cage), within the donor compartment, and within the recipient compartment (Fig. 2A). Particles were loaded for 1 hour to establish

steady-state size distribution (Suppl. Fig. 1A) and sampled three times for 20 seconds totaling 1 minute at each position.

We first characterized particle behavior under ambient room pressure, beginning with the earliest systems, 0 and 1. In system 0, which lacked directional airflow, we observed marked particle loss from both donor and recipient compartments, particularly for particles larger than 4 µm (Fig. 2B-C). System 1, operated with the manufacturer's default airflow settings (8.8 L/min supply; 2.5 L/min exhaust), also showed significant particle depletion (Fig. 2D-E). These findings indicated that the high ventilation rates used for standard animal husbandry, intended to prevent excessive humidity and ammonia and CO_2 accumulation, were incompatible with retention of aerosolized particles. Successful transmission would likely require precise titration of airflow to maintain particle dwell time without compromising animal welfare.

Guided by these results, we next developed system 2A, in which air movement was driven solely by the exhaust fan (2.5 L/min). This modification improved particle retention within both donor and recipient compartments under ambient conditions, especially for particles less than 2µm (Fig. 2F-G).

Inspection of system 1 also revealed a structural limitation: its double-walled stainless-steel barrier created a wide and obstructed path for particle transfer between compartments. To address this, we engineered a new single-walled stainless-steel barrier with larger perforations to reduce physical impedance to airflow. We also sealed the cage to minimize leakage by taping the lid with aluminum tape, adding a rubber gasket along the lid-base junction, and securing the lid with four spring-loaded clamps. The resulting configuration, designated system 2B, was designed to optimize both

airflow continuity and particle containment (Fig. 2H). Under ambient pressure, system 2B achieved particle retention comparable to system 2A, with stable concentrations of particles <2µm in both compartments (Fig. 2I). The similarity between the two systems suggested that the improvements achieved by airflow titration and cage sealing were robust across minor design variations. However, because all prior experiments without transmission had occurred under negative-pressure BSL-3 conditions, further testing under those settings was essential to evaluate real-world performance.

Negative pressure and associated airflow profoundly influence particle retention

Because all Mtb transmission studies must be performed under BSL-3 conditions, the next critical step was to evaluate how negative pressure, an essential safety feature, affects particle movement within the cage systems. To do this, we placed each system inside a custom airtight chamber maintained at the negative-pressure setting used in our ABSL-3 facility (relative negative pressure -0.03 WC) (Fig. 3A). Of note, only system 0 cages were tested at -0.06 WC because the room in which the system 0 cages were maintained during their use for transmission studies was at -0.06 WC, whereas for system 1 and 2B, the animal rack was in a room with -0.03 WC relative negative pressure. Under these conditions, we observed a striking loss of aerosolized particles in both donor and recipient compartments of system 0 (Fig. 3B, C). The unsealed cage design allowed particles to escape through lid gaps and barrier edges, resulting in near-complete depletion of particles across all measured size ranges. System 1 also exhibited substantial particle loss under negative pressure, particularly in the recipient compartment (Fig. 3D, E), indicating that unidirectional airflow alone could not overcome the strong external flow imposed by facility ventilation. System 2A, which

incorporated reduced exhaust flow and a modified barrier, also showed lower particle retention in the recipient compartment (Fig 3F, G). The most dramatic improvement was achieved with system 2B, which combined controlled exhaust flow with cage sealing. Under negative pressure-induced flow, system 2B maintained high concentrations of aerosols within both donor and recipient compartments, demonstrating markedly improved particle retention compared to all previous iterations (Fig. 3H, I).

Together, these results reveal that negative pressure-induced flow profoundly alters internal cage mixing, often removing aerosols before they can traverse from donor to recipient compartments. Through progressive modification of airflow, barrier design, and cage sealing, system 2B successfully counteracted these losses, providing stable particle retention even under the stringent airflow conditions required for BSL-3 containment. This optimized configuration was therefore selected for subsequent transmission experiments.

Biological factors impacting transmission

We next evaluated the impact of environmental variables on transmission efficiency in our optimized cage system. To model movement of bacteria-containing particles, we nebulized a suspension of *Mycobacterium smegmatis,* a non-pathogenic mycobacterial species, in the donor compartment and measured bacterial recovery from air sampled on the recipient side. Recovery of *M. smegmatis* showed a clear dependence on airflow rate, with the highest recovery observed at the lowest exhaust setting of 0.15 L/min (Fig. 4A). This pattern suggested that reduced airflow prolongs particle dwell time within the cage and enhances the likelihood of bacterial transport between compartments.

We then tested if aerosolized bacteria from the donor compartment could deposit into the lungs of naïve guinea pigs housed on the recipient side. We placed individual guinea pigs in the recipient compartment and nebulized a suspension of *M. smegmatis* in the donor compartment for one minute to simulate a cough paroxysm. After 15 minutes of exposure to *M. smegmatis*, we collected and homogenized the lungs of recipient guinea pigs and quantified colony forming units (CFU). All four recipient guinea pigs had recoverable *M. smegmatis* CFU in their lungs (Fig. 4B), demonstrating that aerosolized bacteria generated in the donor compartment were effectively transported and inhaled by recipient animals.

Because humidity strongly influences aerosol dynamics by affecting particle desiccation and settling (Bourouiba, 2021; Li et al., 2021), we next quantified relative humidity (RH) in occupied cages. We housed two guinea pigs (one per compartment) for six days in system 2B cages, and measured RH daily at three exhaust flow rates (2.5, 1.5, and 0.15 L/min). At the lowest airflow rate, humidity rose rapidly, reaching approximately 75 percent by day six (Fig. 4C). Higher airflow rates maintained RH near 65% throughout the experimental, consistent with enhanced air exchange and moisture removal (Fig. 4C). Although lower exhaust flow improved particle transport, the associated increase in humidity was expected to impair aerosol stability and potentially affect animal welfare during long term studies. Based on these considerations, we selected an exhaust flow rate of 2.5 L/min for subsequent Mtb transmission experiments using system 2B.

Mtb transmission under optimized conditions

Having established airflow and environmental parameters that favored particle retention, we next assessed whether these optimized conditions supported Mtb transmission

between guinea pigs. We infected guinea pigs with Mtb (Suppl. Fig 2A) and placed them in the donor compartment of system 2B cages, while naïve guinea pigs were housed in the recipient compartment for a 17-week exposure period. Because guinea pigs develop progressive disease following infection, donor animals were replaced every six weeks to maintain a consistent infectious source.

We monitored for transmission with monthly TST analysis using a two-stage protocol (2000; Jensen et al., 2005; Taylor et al., 2005) by testing animals twice with a 7-day waiting period between doses (Fig. 5A). We also performed TSTs on all donor animals after 4 weeks of infection. Donor animals developed robust TST responses (mean 10 mm; range 6-16 mm), consistent with active infection (Fig. 5B). To define a threshold for positive conversion in recipients, we performed repeated TSTs in unexposed control animals and found that none exceeded 5.5 mm. Using this as a baseline, combined with TST data from Mtb-infected donor animals and uninfected naïve animals, we established a TST cutoff of 6.5 mm to indicate infection (Suppl. Fig 2D-E). Within one month of exposure, one recipient exceeded this threshold, and by week 17, nine of twelve recipient animals demonstrated positive TSTs (Fig. 5B, Suppl. Fig 3).

While TST is a measure of cell-mediated immunity, Mtb exposed individuals also develop humoral responses indicative of exposure or infection (Davies et al., 2023; Davies et al., 2024; Kroon et al., 2020; Lu et al., 2016; Lu et al., 2020; Lu et al., 2019). Thus, to corroborate the TST results with an independent immunologic measure, we quantified serum antibody responses to Mtb antigens representing either complex mixtures (such as PPD) or defined highly immunogenic proteins such as antigen 85B using a bead-based multiplex assay (Suppl. Fig. 4A) (Lu et al., 2019). We calculated the

AUC (area under the curve) for each antigen using a dilution curve and generated ROC (receiver operating characteristic) curves for individual or combination antigen-specific IgGs (Suppl. Fig. 4B-G). Infected donors exhibited strong IgG responses to both antigens, whereas unexposed controls remained negative. Using an ROC predictive probability cutoff of 0.5 for the combined IgG response to antigen 85B and PPD (Suppl. Fig. 4H), eight of twelve recipient animals displayed serologic responses consistent with Mtb exposure (Fig. 5C).

We next examined lung tissues from recipient guinea pigs by blinded histopathology analysis. Compared to unexposed controls, exposed recipients exhibited increased pulmonary inflammation characterized by stage 1 granulomas, intra-alveolar hemorrhage, and small foci of epithelioid macrophages (Fig. 6D-E, Suppl. Fig. 2F-G). Although no culturable Mtb was recovered, the combination of TST conversion, serologic response, and histopathologic evidence indicated that recipient animals had been exposed to and immunologically responded to Mtb.

Together, these results demonstrate that the optimized system 2B configuration supports natural transmission of Mtb between infected and naïve guinea pigs. The integration of controlled airflow, cage sealing, and structural refinement enabled sufficient aerosol retention to permit infection under BSL-3 containment, providing a reproducible experimental model for studying the determinants of airborne TB spread.

DISCUSSION

Our current understanding of TB transmission arises largely from epidemiologic studies of Mtb spread within human populations or from analysis of exhaled aerosols (Fennelly,

2020; Fennelly et al., 2012; Fennelly et al., 2004; Lan et al., 2025; Patterson et al., 2025; Tristao et al., 2025). Experimental validation of these observations has been constrained by the lack of modern animal-to-animal transmission systems. Using a multidisciplinary approach that integrates flow physics, engineering, and infection biology, we developed an optimized guinea pig model that captures the essential features of natural Mtb transmission. This system preserves airborne infectious particles expelled by donor animals and facilitates their transfer to susceptible recipients, thereby enabling mechanistic studies of transmission.

Through iterative optimization, we identified airflow as a key determinant of transmission. Retention of particles within the 1-5 µm range, which can carry Mtb (Fennelly, 2020; Fennelly et al., 2012; Fennelly et al., 2004; Tristao et al., 2025), required balance between airflow rate and containment parameters. Static environments lost particles to the environment and limited aerosol transport, while excessive ventilation air changes eliminated particles before they reached the recipient compartment. By defining the airflow range that allows aerosol particle persistence, we successfully achieved transmission under negative-pressure BSL-3 conditions. Recipient animals mounted measurable immune responses to Mtb antigens and displayed pulmonary inflammation consistent with early infection. These results demonstrate that natural airborne transmission of Mtb can be reconstituted when airflow is tailored to favor airborne particle retention and exposure.

The influence of overall ventilation on infection risk has long been recognized, from the classic studies of Riley and Wells, to modern public health strategies for airborne disease control. The COVID-19 pandemic renewed attention to air exchange rates as a

means of mitigating transmission in hospitals and community settings (Bourouiba, 2020). However, such ventilation strategies pose challenges when modeling infectious disease transmission experimentally. Our results show that both overly static and overly ventilated systems suppress transmission, providing a biophysical explanation for the scarcity of animal-to-animal models since the advent of modern biosafety facilities. In addition, our results provide experimental confirmation that airborne TB transmission can be mitigated with sufficient replenishment of fresh air (Beggs et al., 2003; Escombe et al., 2007b; Granich et al., 1999; Jensen et al., 2005; W.H.O., 2024), as illustrated by our experimental outcomes showing absence of animal-to-animal transmission in systems 0 and 1. By accounting for these aerodynamic constraints, our study establishes a framework for designing experimental systems that control airflow intensity and patterns and can faithfully model airborne pathogen spread under safe laboratory conditions.

The ability to reproduce natural transmission has important implications for tuberculosis biology. Few tools currently exist to test hypotheses about how bacterial, host, and environmental factors interact to shape the transmission cascade. Most experimental systems rely on artificial aerosolization of Mtb to naïve animals (Nuritdinov et al., 2025), human-to-guinea pig exposure systems (Dharmadhikari et al., 2011; Escombe et al., 2007a), or small animal models with unknown correlates to human TB (Gupta et al., 2022; Ramos et al., 2017). The system described here provides a means to investigate transmission directly between infected and naïve animals in a well-characterized model of TB disease. It can be adapted to test how microbial factors such as strain lineage (Coscolla and Gagneux, 2014; Cui et al., 2019; Holt et al., 2018;

Huang et al., 2020; Koleske et al., 2025; Niemann et al., 2010; Yang et al., 2012), lipid composition (Moopanar and Mvubu, 2020; Naqvi et al., 2025; Ruhl et al., 2020), genetic background (Verma et al., 2019) or specific Mtb genes (Mishra et al., 2025) affect transmissibility, and to examine how donor physiology influences aerosol generation and infection probability.

The relationship between respiratory behavior and transmission remains a particularly important question. Recent studies have shown that tidal breathing alone can generate infectious bioaerosols (Dinkele et al., 2022; Dinkele et al., 2024a; Dinkele et al., 2024b), raising debate about the relative contribution of cough to new infections (Patterson and Wood, 2019). Coughing, however, produces more particles than quiet breathing and propels them over longer distances (Bourouiba, 2020; Bourouiba, 2021; Bourouiba et al., 2014; Li et al., 2021; Tristao et al., 2025; Wang et al., 2025). Our prior work identified specific Mtb cell wall glycolipids, sulfolipid-1 and phenolic glycolipid, as sufficient to induce cough in naïve guinea pigs (Naqvi et al., 2025; Ruhl et al., 2020), and guinea pigs infected with Mtb strains lacking both lipids did not cough, despite extensive pulmonary pathology (Ruhl et al., 2020). In the context of the current model, comparing donors that do or do not express these lipids will allow direct testing of how pathogen-encoded factors that trigger cough influence transmission efficiency.

This study has several limitations. Although recipient animals showed consistent immunologic and histologic evidence of exposure, we did not recover culturable Mtb from their lungs. Earlier studies of human-to-guinea pig transmission reported similar findings, and subsequent immunosuppression with dexamethasone revealed latent infection (Dharmadhikari et al., 2011). Extending exposure duration or introducing a

recovery phase with transient immunosuppression may increase bacterial detection in future experiments. Additionally, replacement of moribund donor animals prevented correlation of donor bacterial burden or cough frequency with recipient infection outcomes. Future studies will pair physiologic monitoring of donors with environmental sampling to define the quantitative relationship between aerosol production, bacterial load, and transmission success.

In summary, this work revives a classical model of airborne tuberculosis transmission and adapts it for modern biosafety conditions. Through iterative optimization of cage design and airflow parameters, we demonstrate that airflow governs the transport and retention of infectious particles and determine the likelihood of transmission. This system establishes a reproducible physics-informed platform to investigate the environmental, microbial, and host factors that drive airborne spread of Mtb and to develop novel pharmacological and non-pharmacological transmission blocking interventions.

MATERIALS AND METHODS

Animal studies

Protocols for guinea pig infection and transmission studies were reviewed and approved by the Institutional Animal Care and Use Committee at the University of Texas Southwestern Medical Center (Protocol # 2018-102280-USDA).

Particle transmission

Aerosol particles were generated using a custom-built particle generation system. A syringe pump (Braintree Scientific, MA, USA) delivered EMEM (Suppl. fig 1B)

suspension solution at a flow rate of 0.4 mL/min. Compressed air at 60 psi atomized and dried the aerosols, with a total flow of 21.5 L/min. Relative humidity along the tubing was monitored with a probe (Ahlborn, Germany) and maintained at 48 ± 2%. Continuous aerosol loading into the cage was controlled at 0.3 L/min, while excess flow was vented using a vacuum pump (Gast Manufacturing, MI, USA) regulated by a mass flow controller (MFC; Aalborg Instruments and Controls, NY, USA).

Four case systems were evaluated: System 0, System 1, System 2A, and System 2B. Each consisted of donor and recipient compartments separated by a divider, with 0.3 L/min entering the donor side. Flow conditions varied among tests as summarized in Table 1. Compressed supply air (8.8 L/min) could be directed into the donor side, and exhaust air (2.5 L/min) was regulated using a custom-built laminar flow element connected to the facility vacuum.

Table 1: Flow conditions for cage systems

Testing case	System 0	System 1	System 2A	System 2B
Divider Modification	Plexiglass, double wall	Stainless steel, double wall	Stainless steel, double wall	Stainless steel, single wall
Lid sealing	Off	Off	Off	On
8.8 L/min supply	Off	On	Off	Off
2.5 L/min exhaust	Off	On	On	On

Aerosol particle size distributions were measured on both donor and recipient sides using an Aerodynamic Particle Sizer (APS; Model 3321, TSI, MN, USA). The APS drew 0.3 L/min directly from each sampling site, while dilution air was added through

compressed air controlled by a MFC to achieve the required 5 L/min sampling flow. Before aerosol introduction, clean air was flushed through the cage for 30 min to confirm negligible background particle concentrations. Aerosol particles were then loaded for approximately 1 h to reach steady-state size distributions (Suppl. Fig. 1A). After loading, three 20-second samples were collected per minute, alternating between donor and recipient sides. The particle size boundary was set to 0.8-7μm. Sampling was repeated every 5 min over a 25-min period under both ambient and negative-pressure conditions.

To reproduce biosafety level 3 negative-pressure environments, a custom chamber (24″ × 24″ × 48″) was constructed. An inline duct fan (TerraBloom LLC, CA, USA) regulated airflow, and chamber pressure was monitored continuously using a differential gauge (Dwyer Instruments, Inc., IN, USA), maintained at −0.03 inches of water.

Mycobacterium smegmatis particle transmission

Mycobacterium smegmatis cultures were grown in Middlebrook 7H9 broth (Sigma #M0178) supplemented with 10% OADC, 0.5% glycerol, and 0.05% Tween-80 at 37 °C with shaking (100 rpm). Cultures were diluted to 1 × 10□ CFU/mL in PBS and aerosolized using a Blaustein Atomizing Module (CH Technologies). The atomizer was placed in the donor compartment of the transmission cage, and aerosols were generated for 1 min. After a 2-min delay, air from the recipient compartment was sampled for 30 s using a button sampler (SKC, PA, USA) with a gelatin filter at 10 L/min. The filter was dissolved in PBS and plated on Middlebrook 7H10 agar supplemented with OADC and glycerol. Colonies were counted after overnight incubation to quantify

recovered bacteria. This procedure was repeated at exhaust flow rates of 2.5, 1.5, and 0.15 L/min.

For transmission of *M. smegmatis* to guinea pigs, the atomizer was placed in the donor compartment containing 1×10^5 CFU/mL of *M. smegmatis* in PBS. The recipient compartment contained 2 guinea pigs. Aerosols were generated for 1 min and allowed to pass to the recipient compartment and inhaled by the recipient animals for 15 minutes. Following the 15-minute period, animals were sacrificed and lungs were homogenized in PBS and plated on four 7H10 agar plates per animal to quantify recovered bacteria. This process was repeated for a total of four guinea pigs.

Guinea pig aerosol infection

Donor guinea pigs were infected with *M. tuberculosis* Erdman in three groups on a 6-7 week cycle. Bacteria were cultured in Middlebrook 7H9 broth supplemented with 10% OADC, 0.5% glycerol, and 0.05% Tween-80 at 37 °C using a roller apparatus. Cultures were washed three times with PBS and resuspended, then centrifuged at 500 rpm for 5 min to remove large clumps. The supernatant was sonicated at 90% amplitude for 15-s pulses (Branson Ultrasonics, CT, USA) to generate a single-cell suspension and diluted to 3 × 10□ CFU/mL. The inoculum was aerosolized using a Glas-Col inhalation exposure system (Glas-Col, IN, USA). Two animals per group were sacrificed immediately post-exposure for day-0 CFU quantification by lung plating on 7H11 agar. All animals were weighed weekly, and donors were euthanized seven weeks post-infection.

Transmission experiments and cage modifications

For transmission experiments, male Hartley guinea pigs (Charles River) were used. For system 0, we used a polycarbonate static cage (Tecniplast # 2000P00SU), with a raised lid (Tecniplast #2000P224) covered by a filter top (Tecniplast #2000P400SU) that used conventional static cage top filters (Tecniplast #U1144B420RBOX-300) with a custom designed double walled plexiglass divider perforated with holes for particle movement between compartments. For the transmission experiment, cages were maintained on a stainless-steel rack in our ABSL3. For systems 1 and 2B, we housed animals in an Allentown 1800 15 cage rack (Allentown, NJ, PA). The standard cage bottom (Allentown #315351-1) and external bottle top (Allentown #230347) were used with the following modifications. For both system 1 and 2B, the donor-side exhaust port (right) and recipient-side supply ports (left) were sealed with rubber caps. While for system 1 the supply air was “on”, for system 2B, the supply hose was disconnected from the main air inlet of the rack. For system 2B, a custom stainless-steel cage divider with 102 ventilation holes was fabricated locally to separate donor and recipient animals within each cage. To improve sealing, the underside of the lid was covered with aluminum tape, a 1.6 mm rubber gasket was applied along the lid-base junction, and four 2-inch spring clamps secured the lid once cages were positioned on the rack.

Tuberculin skin test

To determine Mtb exposure, guinea pigs were tested every four weeks using a two-step TST protocol. Animals were anesthetized under 3% isoflurane, and the right or left flank was shaved and cleaned with 70% ethanol. Tuberculin purified protein derivative (PPD; 100 µL of 5 TU, McGuff Medical Products #001079) was injected intradermally. Induration was measured at 24 h and 48 h post-injection. The procedure was repeated

one week later on the opposite flank. Control animals received a single dose of tuberculin at baseline or the same number of total doses (seven) as exposed animals to control for effects of repeated testing.

Serologic analysis

Antigen-specific IgG levels were quantified as previously described with minor modifications (Adhikari et al., 2024; Bates et al., 2022; Lu et al., 2019). Carboxylated microsphere beads (Luminex Corp., Austin, TX, USA) were coupled to protein antigens via covalent NHS-ester linkages using 1-ethyl-3-[3-dimethylaminopropyl] carbodiimide hydrochloride (EDC) and *N*-hydroxysulfosuccinimide (NHS) (Thermo Fisher Scientific, Waltham, MA, USA), following the manufacturer's instructions. MagPlex® Avidin microspheres (Luminex) were conjugated to biotinylated sulfolipid-1 (SL-1) using the manufacturer's protocol.

The following antigens were used: Ag85A (BEI Resources NR-14871), Ag85B (NR-14870), ESAT-6 (NR-49424), CFP-10 (NR-49425), purified protein derivative (PPD; Statens Serum Institute, Copenhagen, Denmark), *M. tuberculosis* H37Rv whole-cell lysate (NR-14822), and *M. tuberculosis* H37Rv cell wall fraction (NR-14828).

Antigen-coupled microspheres (1,000 beads per well) were incubated with diluted guinea pig serum (1:50, 1:250, and 1:1,250) in 96-well Bio-Plex Pro flat-bottom plates (Bio-Rad Laboratories, Hercules, CA, USA) at 4 °C for 16 h. After washing to remove unbound antibodies, antigen-specific IgG was detected using phycoerythrin (PE)-conjugated goat anti-guinea pig IgG (Novus Biologicals, NBP1-74874PE). Beads were incubated with the secondary antibody for 2 h at room temperature, washed with PBS

containing 0.05% Tween-20, and resuspended in PBS. Fluorescence intensity was acquired using a MAGPIX® instrument running xPONENT 4.2 software (Luminex).

Relative antigen-specific IgG levels were quantified as the area under the curve (AUC) calculated from the three serial serum dilutions for each sample.

Receiver operating characteristic (ROC) curves were generated using GraphPad Prism version 10.5 (GraphPad Software, San Diego, CA, USA). Sensitivity and specificity at selected cutoff points, along with 95% confidence intervals, were calculated using logistic regression.

Histologic analysis

At study completion, animals were euthanized, and lungs were collected in 10% neutral-buffered formalin for histopathologic analysis. Fixed tissues were transferred to 70% ethanol and processed by the Histo Pathology Core Facility at UT Southwestern. Paraffin-embedded blocks were sectioned at 5 µm and stained with hematoxylin and eosin. Slides were scanned using a NanoZoomer S60 digital slide scanner, randomized, and blinded prior to evaluation by a pathologist. The number and stage of granulomas were recorded, and pulmonary inflammation was described for each animal. After unblinding, data were compared between naïve and exposed animals using a Mann-Whitney test (GraphPad Prism v10).

ACKNOWLEDGMENTS

The authors would like to thank Cody Ruhl for preliminary experiments, and all members of the Shiloh lab for their support and constructive feedback. We also thank members of the Animal Resources Center at UT Southwestern for providing support

with animal husbandry and the engineering team at Allentown, Inc. for their feedback throughout this project. This work was supported by NIH T32 AI007520 (K.F.N), R21AI181258 (H.O.), R21AI137545 (M.U.S.), R01 AI158688 (M.U.S), R01AI158858 (L.L.L.) and P01 AI159402 (L.B., M.U.S). Financial support was also provided by the Burroughs Wellcome Fund 1017894 (M.U.S). Michael Shiloh and Lenette Lu would also like to acknowledge generous support from the Disease Oriented Clinical Scholar program at UT Southwestern Medical Center.

AUTHOR CONTRIBUTIONS

Conceptualization, K.F.N, L.B. and M.U.S. Formal Analysis, K.F.N, Y.G., D.S., P.L., S.W., A.M., B.M.E., L.L., H.O., L.B. and M.U.S. Funding Acquisition, L.B. and M.U.S. Investigation, K.F.N, Y.G., D.S., P.L., S.W., B.R.S.D., V.A.E., A.E.M., B.M.E., L.L. Project Administration, K.F.N and M.U.S. Resources, H.O., M.U.S. Validation, K.F.N, Y.G., D.S., P.L., A.E.M. Supervision, L.L.L., H.O., L.B. and M.U.S. Writing- original draft, K.F.N and M.U.S. Writing-Review and Editing, all authors.

DECLARATION OF COMPETING INTERESTS

All authors declare that they have no competing interests.

References

2000. Targeted tuberculin testing and treatment of latent tuberculosis infection. This official statement of the American Thoracic Society was adopted by the ATS Board of Directors, July 1999. This is a Joint Statement of the American Thoracic Society (ATS) and the Centers for Disease Control and Prevention (CDC). This statement was endorsed by the Council of the Infectious Diseases Society of America. (IDSA), September 1999, and the sections of this statement. *Am J Respir Crit Care Med* 161:S221-247. https://www.ncbi.nlm.nih.gov/pubmed/10764341.

2024. Global Tuberculosis Report 2024. *Geneva:World Health Organization* Licence: CC BY-NC-SA 3.0 IGO:

Adhikari, E.H., P. Lu, Y.J. Kang, A.R. McDonald, J.E. Pruszynski, T.A. Bates, S.K. McBride, M. Trank-Greene, F.G. Tafesse, and L.L. Lu. 2024. Diverging Maternal and Cord Antibody Functions From SARS-CoV-2 Infection and Vaccination in Pregnancy. *J Infect Dis* 229:462-472. PMC10873180. https://www.ncbi.nlm.nih.gov/pubmed/37815524.

Bates, T.A., P. Lu, Y.J. Kang, D. Schoen, M. Thornton, S.K. McBride, C. Park, D. Kim, W.B. Messer, M.E. Curlin, F.G. Tafesse, and L.L. Lu. 2022. BNT162b2-induced neutralizing and non-neutralizing antibody functions against SARS-CoV-2 diminish with age. *Cell Rep* 41:111544. PMC9533669. https://www.ncbi.nlm.nih.gov/pubmed/36252569.

Beggs, C.B., C.J. Noakes, P.A. Sleigh, L.A. Fletcher, and K. Siddiqi. 2003. The transmission of tuberculosis in confined spaces: an analytical review of alternative epidemiological models. *Int J Tuberc Lung Dis* 7:1015-1026. https://www.ncbi.nlm.nih.gov/pubmed/14598959.

Bourouiba, L. 2020. Turbulent Gas Clouds and Respiratory Pathogen Emissions: Potential Implications for Reducing Transmission of COVID-19. *JAMA* 323:1837-1838. https://www.ncbi.nlm.nih.gov/pubmed/32215590.

Bourouiba, L. 2021. Fluid Dynamics of Respiratory Infectious Diseases. *Annu Rev Biomed Eng* 23:547-577. https://www.ncbi.nlm.nih.gov/pubmed/34255991.

Bourouiba, L., E. Dehandschoewercker, and J.W.M. Bush. 2014. Violent expiratory events: on coughing and sneezing. *J Fluid Mech* 745:537-563. <Go to ISI>://WOS:000333907700023.

Brown, C.D., B.M. Lee, H. Liu, A. Wu, A. Tellez, H. Zou, P. Singh, K. Saito, S. Mishra, M. Brown, A. Saleh, N. Odjourian, M. Cristaldo, M. Gan, Q. Liu, M. Gengenbacher, S. Darst, E. Campbell, C. Nathan, and K.Y. Rhee. 2025. Desiccation-induced DNA damage facilitates drug resistance in Mycobacterium tuberculosis. *bioRxiv* PMC12157685. https://www.ncbi.nlm.nih.gov/pubmed/40501622.

Canning, B.J. 2008. The cough reflex in animals: relevance to human cough research. *Lung* 186 Suppl 1:S23-28. PMC2882536. https://www.ncbi.nlm.nih.gov/pubmed/18080711.

Coscolla, M., and S. Gagneux. 2014. Consequences of genomic diversity in Mycobacterium tuberculosis. *Semin Immunol* 26:431-444. PMC4314449. https://www.ncbi.nlm.nih.gov/pubmed/25453224.

Cui, Z., D. Lin, V. Chongsuvivatwong, E.A. Graviss, A. Chaiprasert, P. Palittapongarnpim, M. Lin, J. Ou, and J. Zhao. 2019. Hot and Cold Spot Areas of Household Tuberculosis Transmission in Southern China: Effects of Socio-Economic Status and Mycobacterium tuberculosis Genotypes. *Int J Environ Res Public Health* 16:PMC6572207. https://www.ncbi.nlm.nih.gov/pubmed/31137811.

Davies, L.R.L., M.T. Smith, D. Cizmeci, S. Fischinger, J. Shih-Lu Lee, L.L. Lu, E.D. Layton, A.D. Grant, K. Fielding, C.M. Stein, W.H. Boom, T.R. Hawn, S.M. Fortune, R.S. Wallis, G.J. Churchyard, G. Alter, and C. Seshadri. 2023. IFN-gamma independent markers of Mycobacterium tuberculosis exposure among male South African gold miners. *EBioMedicine* 93:104678. PMC10320233. https://www.ncbi.nlm.nih.gov/pubmed/37379655.

Davies, L.R.L., C. Wang, P. Steigler, K.A. Bowman, S. Fischinger, M. Hatherill, M. Fisher, S.K. Mbandi, M. Rodo, T.H.M. Ottenhoff, H.M. Dockrell, J.S. Sutherland, H. Mayanja-Kizza, W.H. Boom, G. Walzl, S.H.E. Kaufmann, E. Nemes, T.J. Scriba, D. Lauffenburger, G. Alter, and S.M. Fortune. 2024. Age and sex influence antibody profiles associated with tuberculosis progression. *Nat Microbiol* 9:1513-1525. PMC11153143. https://www.ncbi.nlm.nih.gov/pubmed/38658786.

Dharmadhikari, A.S., R.J. Basaraba, M.L. Van Der Walt, K. Weyer, M. Mphahlele, K. Venter, P.A. Jensen, M.W. First, S. Parsons, D.N. McMurray, I.M. Orme, and E.A. Nardell. 2011. Natural infection of guinea pigs exposed to patients with highly drug-resistant tuberculosis. *Tuberculosis (Edinb)* 91:329-338. PMC3339040. https://www.ncbi.nlm.nih.gov/pubmed/21478054.

Dinkele, R., S. Gessner, A. McKerry, B. Leonard, J. Leukes, R. Seldon, D.F. Warner, and R. Wood. 2022. Aerosolization of Mycobacterium tuberculosis by Tidal Breathing. *Am J Respir Crit Care Med* 206:206-216. PMC9887416. https://www.ncbi.nlm.nih.gov/pubmed/35584342.

Dinkele, R., S. Gessner, B. Patterson, A. McKerry, Z. Hoosen, A. Vazi, R. Seldon, A. Koch, D.F. Warner, and R. Wood. 2024a. Persistent Mycobacterium tuberculosis bioaerosol release in a tuberculosis-endemic setting. *iScience* 27:110731. PMC11414687. https://www.ncbi.nlm.nih.gov/pubmed/39310776.

Dinkele, R., P.Y. Khan, and D.F. Warner. 2024b. Mycobacterium tuberculosis transmission: the importance of precision. *Lancet Infect Dis* 24:679-681. https://www.ncbi.nlm.nih.gov/pubmed/38527472.

Donald, P.R., A.H. Diacon, C. Lange, A.M. Demers, F. von Groote-Bidlingmaier, and E. Nardell. 2018. Droplets, dust and guinea pigs: an historical review of tuberculosis transmission research, 1878-1940. *Int J Tuberc Lung Dis* 22:972-982. https://www.ncbi.nlm.nih.gov/pubmed/30092861.

Duguid, J.P. 1946. The size and the duration of air-carriage of respiratory droplets and droplet-nuclei. *J Hyg (Lond)* 44:471-479. PMC2234804. https://www.ncbi.nlm.nih.gov/pubmed/20475760.

Escombe, A.R., C. Oeser, R.H. Gilman, M. Navincopa, E. Ticona, C. Martinez, L. Caviedes, P. Sheen, A. Gonzalez, C. Noakes, D.A. Moore, J.S. Friedland, and C.A. Evans. 2007a. The detection of airborne transmission of tuberculosis from HIV-infected patients, using an in vivo air sampling model. *Clin Infect Dis* 44:1349-1357. PMC2912511. https://www.ncbi.nlm.nih.gov/pubmed/17443474.

Escombe, A.R., C.C. Oeser, R.H. Gilman, M. Navincopa, E. Ticona, W. Pan, C. Martinez, J. Chacaltana, R. Rodriguez, D.A. Moore, J.S. Friedland, and C.A. Evans. 2007b. Natural ventilation for the prevention of airborne contagion. *PLoS Med* 4:e68. PMC1808096. https://www.ncbi.nlm.nih.gov/pubmed/17326709.

Fennelly, K.P. 2020. Particle sizes of infectious aerosols: implications for infection control. *Lancet Respir Med* 8:914-924. PMC7380927. https://www.ncbi.nlm.nih.gov/pubmed/32717211.

Fennelly, K.P., E.C. Jones-Lopez, I. Ayakaka, S. Kim, H. Menyha, B. Kirenga, C. Muchwa, M. Joloba, S. Dryden-Peterson, N. Reilly, A. Okwera, A.M. Elliott, P.G. Smith, R.D. Mugerwa, K.D. Eisenach, and J.J. Ellner. 2012. Variability of infectious aerosols produced during coughing by patients with pulmonary tuberculosis. *Am J Respir Crit Care Med* 186:450-457. PMC3443801. https://www.ncbi.nlm.nih.gov/pubmed/22798319.

Fennelly, K.P., J.W. Martyny, K.E. Fulton, I.M. Orme, D.M. Cave, and L.B. Heifets. 2004. Cough-generated aerosols of Mycobacterium tuberculosis: a new method to study infectiousness. *Am J Respir Crit Care Med* 169:604-609. http://www.ncbi.nlm.nih.gov/pubmed/14656754.

Granich, R., N.J. Binkin, W.R. Jarvis, P.M. Simone, H.L. Rieder, M.A. Espinal, and J. Kumaresan. 1999. Guidelines for the prevention of tuberculosis in health care facilities in resource-limited settings. World health organization (WHO),

Gupta, T., N. Somanna, T. Rowe, M. LaGatta, S. Helms, S.O. Owino, T. Jelesijevic, S. Harvey, W. Jacobs, T. Voss, K. Sakamoto, C. Day, C. Whalen, R. Karls, B. He, S.M. Tompkins, A. Bakre, T. Ross, and F.D. Quinn. 2022. Ferrets as a model for tuberculosis transmission. *Front Cell Infect Microbiol* 12:873416. PMC9425069. https://www.ncbi.nlm.nih.gov/pubmed/36051240.

Holt, K.E., P. McAdam, P.V.K. Thai, N.T.T. Thuong, D.T.M. Ha, N.N. Lan, N.H. Lan, N.T.Q. Nhu, H.T. Hai, V.T.N. Ha, G. Thwaites, D.J. Edwards, A.P. Nath, K. Pham,

D.B. Ascher, J. Farrar, C.C. Khor, Y.Y. Teo, M. Inouye, M. Caws, and S.J. Dunstan. 2018. Frequent transmission of the Mycobacterium tuberculosis Beijing lineage and positive selection for the EsxW Beijing variant in Vietnam. *Nat Genet* 50:849-856. PMC6143168. https://www.ncbi.nlm.nih.gov/pubmed/29785015.

Huang, C.C., A.L. Chu, M.C. Becerra, J.T. Galea, R. Calderon, C. Contreras, R. Yataco, Z. Zhang, L. Lecca, and M.B. Murray. 2020. Mycobacterium tuberculosis Beijing Lineage and Risk for Tuberculosis in Child Household Contacts, Peru. *Emerg Infect Dis* 26:568-578. PMC7045848. https://www.ncbi.nlm.nih.gov/pubmed/32091363.

Jensen, P.A., L.A. Lambert, M.F. Iademarco, R. Ridzon, and Cdc. 2005. Guidelines for preventing the transmission of Mycobacterium tuberculosis in health-care settings, 2005. *MMWR Recomm Rep* 54:1-141. https://www.ncbi.nlm.nih.gov/pubmed/16382216.

Koch, R. 1882. The etiology of tuberculosis. *The germ theory of disease* 109-115.

Koch, R. 1912. Gesammelte Werke von Robt. Koch. *Leipsic* 512.

Koleske, B., C. Schill, S. Rajagopalan, S. Shee, Y.B. Martinez-Martinez, M. Gupta, J. Shen, W.R. Jacobs, Jr., and W.R. Bishai. 2025. Loss of the PPE71-esxX-esxY-PPE38 locus drives adaptive transcriptional responses and hypervirulence of Mycobacterium tuberculosis lineage 2. *Sci Adv* 11:eadw5194. PMC12219505. https://www.ncbi.nlm.nih.gov/pubmed/40601738.

Kroon, E.E., C.J. Kinnear, M. Orlova, S. Fischinger, S. Shin, S. Boolay, G. Walzl, A. Jacobs, R.J. Wilkinson, G. Alter, E. Schurr, E.G. Hoal, and M. Moller. 2020. An observational study identifying highly tuberculosis-exposed, HIV-1-positive but persistently TB, tuberculin and IGRA negative persons with M. tuberculosis specific antibodies in Cape Town, South Africa. *EBioMedicine* 61:103053. PMC7648124. https://www.ncbi.nlm.nih.gov/pubmed/33038764.

Lan, Y., I. Rancu, M.H. Chitwood, B. Sobkowiak, K. Nyhan, H.H. Lin, C.Y. Wu, B. Mathema, T.S. Brown, C. Colijn, J.L. Warren, and T. Cohen. 2025. Integrating genomic and spatial analyses to describe tuberculosis transmission: a scoping review. *Lancet Microbe* 6:101094. PMC12371702. https://www.ncbi.nlm.nih.gov/pubmed/40228509.

Li, H., F.Y. Leong, G. Xu, C.W. Kang, K.H. Lim, B.H. Tan, and C.M. Loo. 2021. Airborne dispersion of droplets during coughing: a physical model of viral transmission. *Sci Rep* 11:4617. PMC7907382. https://www.ncbi.nlm.nih.gov/pubmed/33633316.

Loudon, R.G., and R.M. Roberts. 1968. Singing and the dissemination of tuberculosis. *Am Rev Respir Dis* 98:297-300. https://www.ncbi.nlm.nih.gov/pubmed/5667756.

Loudon, R.G., and S.K. Spohn. 1969. Cough frequency and infectivity in patients with pulmonary tuberculosis. *Am Rev Respir Dis* 99:109-111. https://www.ncbi.nlm.nih.gov/pubmed/5762102.

Lu, L.L., A.W. Chung, T.R. Rosebrock, M. Ghebremichael, W.H. Yu, P.S. Grace, M.K. Schoen, F. Tafesse, C. Martin, V. Leung, A.E. Mahan, M. Sips, M.P. Kumar, J. Tedesco, H. Robinson, E. Tkachenko, M. Draghi, K.J. Freedberg, H. Streeck, T.J. Suscovich, D.A. Lauffenburger, B.I. Restrepo, C. Day, S.M. Fortune, and G. Alter. 2016. A Functional Role for Antibodies in Tuberculosis. *Cell* 167:433-443 e414. PMC5526202. https://www.ncbi.nlm.nih.gov/pubmed/27667685.

Lu, L.L., J. Das, P.S. Grace, S.M. Fortune, B.I. Restrepo, and G. Alter. 2020. Antibody Fc Glycosylation Discriminates Between Latent and Active Tuberculosis. *J Infect Dis* 222:2093-2102. PMC7661770. https://www.ncbi.nlm.nih.gov/pubmed/32060529.

Lu, L.L., M.T. Smith, K.K.Q. Yu, C. Luedemann, T.J. Suscovich, P.S. Grace, A. Cain, W.H. Yu, T.R. McKitrick, D. Lauffenburger, R.D. Cummings, H. Mayanja-Kizza, T.R. Hawn, W.H. Boom, C.M. Stein, S.M. Fortune, C. Seshadri, and G. Alter. 2019. IFN-gamma-independent immune markers of Mycobacterium tuberculosis exposure. *Nat Med* 25:977-987. PMC6559862. https://www.ncbi.nlm.nih.gov/pubmed/31110348.

Lurie, M.B. 1930a. Experimental Epidemiology of Tuberculosis : Air-Borne Contagion of Tuberculosis in an Animal Room. *J Exp Med* 51:743-751. PMC2131796. https://www.ncbi.nlm.nih.gov/pubmed/19869724.

Lurie, M.B. 1930b. Experimental Epidemiology of Tuberculosis : The Effect of Eliminating Exposure to Enteric Infection on the Incidence and Course of Tuberculosis Acquired by Normal Guinea Pigs Confined with Tuberculous Cage Mates. *J Exp Med* 51:753-768. PMC2131786. https://www.ncbi.nlm.nih.gov/pubmed/19869725.

Lurie, M.B. 1930c. Experimental Epidemiology of Tuberculosis : The Route of Infection in Naturally Acquired Tuberculosis of the Guinea Pig. *J Exp Med* 51:769-776. PMC2131790. https://www.ncbi.nlm.nih.gov/pubmed/19869726.

Mangura, B.T., E.C. Napolitano, M.R. Passannante, R.J. McDonald, and L.B. Reichman. 1998. Mycobacterium tuberculosis miniepidemic in a church gospel choir. *Chest* 113:234-237. https://www.ncbi.nlm.nih.gov/pubmed/9440596.

Mazzone, S.B., N. Mori, and B.J. Canning. 2005. Synergistic interactions between airway afferent nerve subtypes regulating the cough reflex in guinea-pigs. *J Physiol* 569:559-573. PMC1464254. https://www.ncbi.nlm.nih.gov/pubmed/16051625.

Mishra, S., P.R. Singh, X. Hu, L. Lopez-Quezada, A. Jinich, R. Jahn, L. Geurts, N. Shen, M.A. DeJesus, T. Hartman, K. Rhee, M. Zimmerman, V. Dartois, R.M. Jones, X. Jiang, R. Almada-Monter, L. Bourouiba, and C. Nathan. 2025. Candidate transmission survival genome of Mycobacterium tuberculosis. *Proc Natl Acad Sci U S A* 122:e2425981122. PMC11912377. https://www.ncbi.nlm.nih.gov/pubmed/40053362.

Moopanar, K., and N.E. Mvubu. 2020. Lineage-specific differences in lipid metabolism and its impact on clinical strains of Mycobacterium tuberculosis. *Microb Pathog* 146:104250. https://www.ncbi.nlm.nih.gov/pubmed/32407863.

Naqvi, K.F., L.L. Warden, J.H.M. van Dijk, D.K. Naik, F. de Jesus Espinosa-Becerra, I.M. Okolie, V.V.F. Verhoeks, K.C. Rahlwes, C.P. Xavier, J.D.C. Codee, T.J. Price, and M.U. Shiloh. 2025. Mycobacterial Phenolic Glycolipid Triggers ATP-Mediated Neuronal P2X3 Signaling and Cough. *bioRxiv* PMC12248122. https://www.ncbi.nlm.nih.gov/pubmed/40654771.

Nardell, E.A. 1999. Air sampling for tuberculosis- homage to the lowly guinea pig. *Chest* 116:1143-1145. https://www.ncbi.nlm.nih.gov/pubmed/10531196.

Niemann, S., R. Diel, G. Khechinashvili, M. Gegia, N. Mdivani, and Y.W. Tang. 2010. Mycobacterium tuberculosis Beijing lineage favors the spread of multidrug-resistant tuberculosis in the Republic of Georgia. *J Clin Microbiol* 48:3544-3550. PMC2953096. https://www.ncbi.nlm.nih.gov/pubmed/20702677.

Nuritdinov, F., J. Woo, M.J. Schmidt, N.M. Odjourian, M. Cristaldo, M. Dougher, R. Antilus-Sainte, T. Heldt, K. Rhee, L. Bourouiba, and M. Gengenbacher. 2025. Experimental system enables studies of Mycobacterium tuberculosis during aerogenic transmission. *mBio* 16:e0095825. PMC12506124. https://www.ncbi.nlm.nih.gov/pubmed/40853127.

Orme, I.M., and D.J. Ordway. 2016. Mouse and Guinea Pig Models of Tuberculosis. *Microbiol Spectr* 4:https://www.ncbi.nlm.nih.gov/pubmed/27726797.

Patterson, B., S. Hermans, R. Wood, and F. Cobelens. 2025. Quantification of tuberculosis exposure in a high-burdened setting. *Sci Rep* 15:22687. PMC12218470. https://www.ncbi.nlm.nih.gov/pubmed/40595677.

Patterson, B., and R. Wood. 2019. Is cough really necessary for TB transmission? *Tuberculosis (Edinb)* 117:31-35. PMC6688829. https://www.ncbi.nlm.nih.gov/pubmed/31378265.

Perla, D. 1927a. Experimental Epidemiology of Tuberculosis. *J Exp Med* 45:209-226. PMC2131270. https://www.ncbi.nlm.nih.gov/pubmed/19869247.

Perla, D. 1927b. Experimental Epidemiology of Tuberculosis : The Elimination of Tubercle Bacilli in the Feces, Bile, and Urine of Infected Guinea Pigs. *J Exp Med* 45:1025-1035. PMC2131157. https://www.ncbi.nlm.nih.gov/pubmed/19869302.

Podell, B.K., D.F. Ackart, A. Obregon-Henao, S.P. Eck, M. Henao-Tamayo, M. Richardson, I.M. Orme, D.J. Ordway, and R.J. Basaraba. 2014. Increased severity of tuberculosis in Guinea pigs with type 2 diabetes: a model of diabetes-tuberculosis comorbidity. *Am J Pathol* 184:1104-1118. PMC3969993. https://www.ncbi.nlm.nih.gov/pubmed/24492198.

Ramos, L., A. Obregon-Henao, M. Henao-Tamayo, R. Bowen, J.K. Lunney, and M. Gonzalez-Juarrero. 2017. The minipig as an animal model to study Mycobacterium tuberculosis infection and natural transmission. *Tuberculosis (Edinb)* 106:91-98. PMC5611812. https://www.ncbi.nlm.nih.gov/pubmed/28802411.

Riley, R.L. 2001. What nobody needs to know about airborne infection. *Am J Respir Crit Care Med* 163:7-8. https://www.ncbi.nlm.nih.gov/pubmed/11208616.

Riley, R.L., C.C. Mills, F. O'Grady, L.U. Sultan, F. Wittstadt, and D.N. Shivpuri. 1962. Infectiousness of air from a tuberculosis ward. Ultraviolet irradiation of infected air: comparative infectiousness of different patients. *Am Rev Respir Dis* 85:511-525. https://www.ncbi.nlm.nih.gov/pubmed/14492300.

Riley, R.L., W.F. Wells, C.C. Mills, W. Nyka, and R.L. McLean. 1957. Air hygiene in tuberculosis: quantitative studies of infectivity and control in a pilot ward. *Am Rev Tuberc* 75:420-431. https://www.ncbi.nlm.nih.gov/pubmed/13403171.

Ruhl, C.R., B.L. Pasko, H.S. Khan, L.M. Kindt, C.E. Stamm, L.H. Franco, C.C. Hsia, M. Zhou, C.R. Davis, T. Qin, L. Gautron, M.D. Burton, G.L. Mejia, D.K. Naik, G. Dussor, T.J. Price, and M.U. Shiloh. 2020. Mycobacterium tuberculosis Sulfolipid-1 Activates Nociceptive Neurons and Induces Cough. *Cell* 181:293-305 e211. PMC7102531. https://www.ncbi.nlm.nih.gov/pubmed/32142653.

Singh, P.R., S. Mishra, A. Jinich, X. Jiang, F. Tsang, M. DeJesus, K.Y. Rhee, R.J. Kaner, P.L. Leopold, R.G. Crystal, and C. Nathan. 2025. Genes required for Mycobacterium tuberculosis to survive the transition from aerosol to pulmonary alveolar lining fluid and early infection in a model of transmission. *bioRxiv* PMC12458190. https://www.ncbi.nlm.nih.gov/pubmed/41000987.

Stoltz, A., R.R. Nathavitharana, E. de Kock, V. Ueckermann, P. Jensen, C.M. Mendel, M. Spigelman, and E.A. Nardell. 2025. Estimating the Early Transmission Inhibition of New Treatment Regimens for Drug-Resistant Tuberculosis. *J Infect Dis* 232:143-151. PMC12308646. https://www.ncbi.nlm.nih.gov/pubmed/39789858.

Taylor, Z., C.M. Nolan, H.M. Blumberg, S. American Thoracic, C. Centers for Disease, Prevention, and A. Infectious Diseases Society of. 2005. Controlling tuberculosis in the United States. Recommendations from the American Thoracic Society, CDC, and the Infectious Diseases Society of America. *MMWR Recomm Rep* 54:1-81. https://www.ncbi.nlm.nih.gov/pubmed/16267499.

Tristao, T.C., M.A.M. Ferreira, P.S. de Almeida Junior, L.G.S. Castellani, M.N. Brunetti, E.C. Jones-Lopez, K.P. Fennelly, M.R. Barer, C.H. Fantecelle, S.A. Morellato, D.J. Hadad, J.J. Ellner, R. Dietze, and M. Palaci. 2025. Dynamic of infectious aerosols generated by cough from patients with pulmonary tuberculosis. *J Aerosol Sci* 189:PMC12237428. https://www.ncbi.nlm.nih.gov/pubmed/40635785.

Turner, R.D., and G.H. Bothamley. 2015. Cough and the transmission of tuberculosis. *J Infect Dis* 211:1367-1372. http://www.ncbi.nlm.nih.gov/pubmed/25387581.

Verma, S., K. Bhatt, A. Lovey, R. Ribeiro-Rodrigues, J. Durbin, E.C. Jones-Lopez, M. Palaci, S.A. Vinhas, D. Alland, R. Dietze, J.J. Ellner, and P. Salgame. 2019. Transmission phenotype of Mycobacterium tuberculosis strains is mechanistically linked to induction of distinct pulmonary pathology. *PLoS Pathog* 15:e1007613. PMC6422314. https://www.ncbi.nlm.nih.gov/pubmed/30840702.

W.H.O. 2024. Global technical consultation report on proposed terminology for pathogens that transmit through the air. In Geneva: World Health Organization.

Wang, C., J. Xu, H. Zhai, L.K. So, and H. Guo. 2025. Mapping full-range infection transmission from speaking, coughing, and sneezing in indoor environments and its impact on social distancing. *J Hazard Mater* 490:137782. https://www.ncbi.nlm.nih.gov/pubmed/40022917.

Wells, W.F. 1955. Airborne Contagion and Air Hygiene: An Ecological Study of Droplet Infections. Harvard University Press, 423 pp.

Wells, W.F., H.L. Ratcliffe, and C. Grumb. 1948. On the mechanics of droplet nuclei infection; quantitative experimental air-borne tuberculosis in rabbits. *Am J Hyg* 47:11-28. https://www.ncbi.nlm.nih.gov/pubmed/18921435.

Yang, C., T. Luo, G. Sun, K. Qiao, G. Sun, K. DeRiemer, J. Mei, and Q. Gao. 2012. Mycobacterium tuberculosis Beijing strains favor transmission but not drug resistance in China. *Clin Infect Dis* 55:1179-1187. PMC3466095. https://www.ncbi.nlm.nih.gov/pubmed/22865872.

Figure legends

Figure 1: Airflow Modifications of Preliminary Transmission Systems (A) Experimental scheme for 12-month transmission studies. Blue ticks indicate when new donor groups were added to cages and stars denote when TSTs were performed. (B) System 0 cage set up with static airflow and plexiglass divider between donor and recipient compartments. (C) 15 cage rack as available by Allentown, Inc. (D) System 1 cage set up. Donor side is connected to supply hose which delivers 8.8 LPM into the cage. Air then passes through a stainless-steel divider to recipient compartment and is exhausted at 2.5 LPM. (E) Modifications to cage rack include plugging the exhaust port on the donor side and supply port on the recipient side to drive unidirectional airflow. (F) Smoke test to confirm unidirectional movement of air within system 1. See also supplemental movie 1.

Figure 2: Particle movement driven by airflow under ambient pressure. (A) Experimental overview of particle transport. Cage systems are connected to supply air (where applicable) and exhaust vacuum to control airflow within the cages. Particles are introduced to the donor compartment using a particle generator. An APS particle sampler collects particles upstream before entering the cage, in the donor and recipient compartments. (B-C) Schematic and particle sampling of System 0 under static flow conditions. (D-E) Schematic and particle sampling of System 1 with supply air set to 8.8 LPM and exhaust to 2.5 LPM. Dashed line indicates unsealed cage lid. (F) System 2A schematic with air supply removed (0LPM) and exhaust set to 2.5 LPM. (G) Particle transport within system 2A. (H-I) Schematic and particle transport of system 2B modified to include cage lid sealing (solid line) and a single stainless-steel barrier. All

particle transport results are represented as number of particles per cubic centimeter of air (#/cc) in the size range of 0.8-7 µm. Sampling of particles includes upstream (red) before entering the cage, in the donor compartment (blue) and the recipient compartment (black).

Figure 3: Negative pressure influences retention of particles within cage systems. (A) Experimental set-up of particle transport where cage systems are placed inside a custom chamber under negative pressure (-0.03 WC). (B-C) System 0 cage design and particle movement within cage system while under negative pressure. (D-E) Addition of unidirectional airflow in system 1 design and particle transport within system 1. Dashed line indicates unsealed cage lid. (F-G) Schematic of system 2A with airflow driven by the exhaust port (2.5LPM) and particle transport under negative pressure conditions. (H-I) System 2B schematic with modified cage lid sealing (solid line) and single cage barrier and particle transport within system 2B. All particle transport results are represented as number of particles per cubic centimeter of air (#/cc) in the size range of 0.8-7 µm. Sampling includes upstream (red) before entering the cage, in the donor compartment (blue) and the recipient compartment (black).

Figure 4: Optimization of biological factors which influence transmission efficiency. (A) Recovery of particles containing *M. smegmatis* from the recipient compartment using a low-flow button sampler at varying exhaust flow rates (0.15, 1.5 and 2.5 L/min). (B) Nebulization of *M. smegmatis* in the donor compartment and recovery of bacteria from lungs of recipient guinea pigs in system 2B cages. Colony forming units (CFU) quantified from lung homogenates plated across four agar plates from four different guinea pigs. Each point represents CFU on an individual plate. (C) Humidity

accumulation during guinea pig housing in system 2B cages. Relative humidity (%) in three system 2B cages with guinea pigs housed in each compartment (two per cage) across 6 days. Three different exhaust flowrates tested include 0.15, 1.5, and 2.5 L/min. Cages were changed at day 4 for all flowrates.

Figure 5: Transmission of Mtb in an optimized cage system. (A) Experimental timeline for 17-week transmission study. Blue ticks indicate when new donor groups were added to the cages. Monthly TSTs using a prime/boost strategy are noted as filled stars (prime dose) and open stars (boost dose). (B) TST measurements for recipient animals throughout the exposure period. Any responses above 6.5 (dashed line) are considered positive. (C) Predicted probability of Mtb exposure based on serum antigen 85B and PPD IgG levels. Values above 0.5 (dashed line) are predicted positive in the donor, naïve, recipient and TST control groups. (D) Quantification of stage 1 granulomata in naïve and recipient lung sections. (E) Representative hematoxylin and eosin staining of lung section from naïve and recipient groups. Inflammatory collection (naïve) and stage 1 granuloma (recipient) at 20x. p-values calculated by one-way ANOVA for multiple comparisons or Mann-Whitney for comparison between two groups. ns=not significant, *=$p<0.05$, **= $p<0.01$, ***=$p<0.001$, ****=$p<0.0001$.

Supplemental Figure 1: Particle generation within cage systems. (A) Concentration equilibrium within cage systems from 6 to 84 minutes of continuous generation. (B) chemical composition of EMEM used for particle generation.

Supplemental Figure 2: Animal characteristics of transmission study (A) Lung CFU directly after aerosol infection (day 0) for donor groups 1,2, and 3. (B) Weight tracking of donor guinea pigs over 7 weeks (group 1 and 2) and 5 weeks for group 3. (C) Weight

tracking of recipient guinea pigs throughout 17-week exposure period. (D) TST measurement in TST control guinea pigs given 7 doses of tuberculin. (E) TST measurement in naïve guinea pigs given one prime and boost dose of tuberculin. Dashed line denotes cut-off (6.5 mm) for positive responses. (F) Hematoxylin and eosin staining of lung sections from 8 naïve animals used for histopathology analysis. (G) Lung sections from 12 recipient animals stained with hematoxylin and eosin for histology analysis.

Supplemental Figure 3: TST measurements of individual recipient guinea pigs. TST measurements for each recipient guinea pig (#1-12) across the exposure period. Any values above 6.5 mm (dashed line) are considered positive. Recordings include the prime and boost dose of tuberculin.

Supplemental Figure 4: Serum antibody levels of guinea pigs. (A) experimental design of bead-based serum antibody quantification. (B) Area under the curve (AUC) of SL-1 specific IgG for donor, naïve, recipient, and TST control groups. Receiver operation characteristic (ROC) curve predictive power (%) for both positive and negative values based on SL-1 antigen specific IgG. (C-G) AUC and ROC curves for cell wall, whole cell lysate, ESAT6 CFP10, PPD, and Antigen 85B specific IgG. (H) ROC curve for combined antigen 85B and PPD IgG.

Figure 1

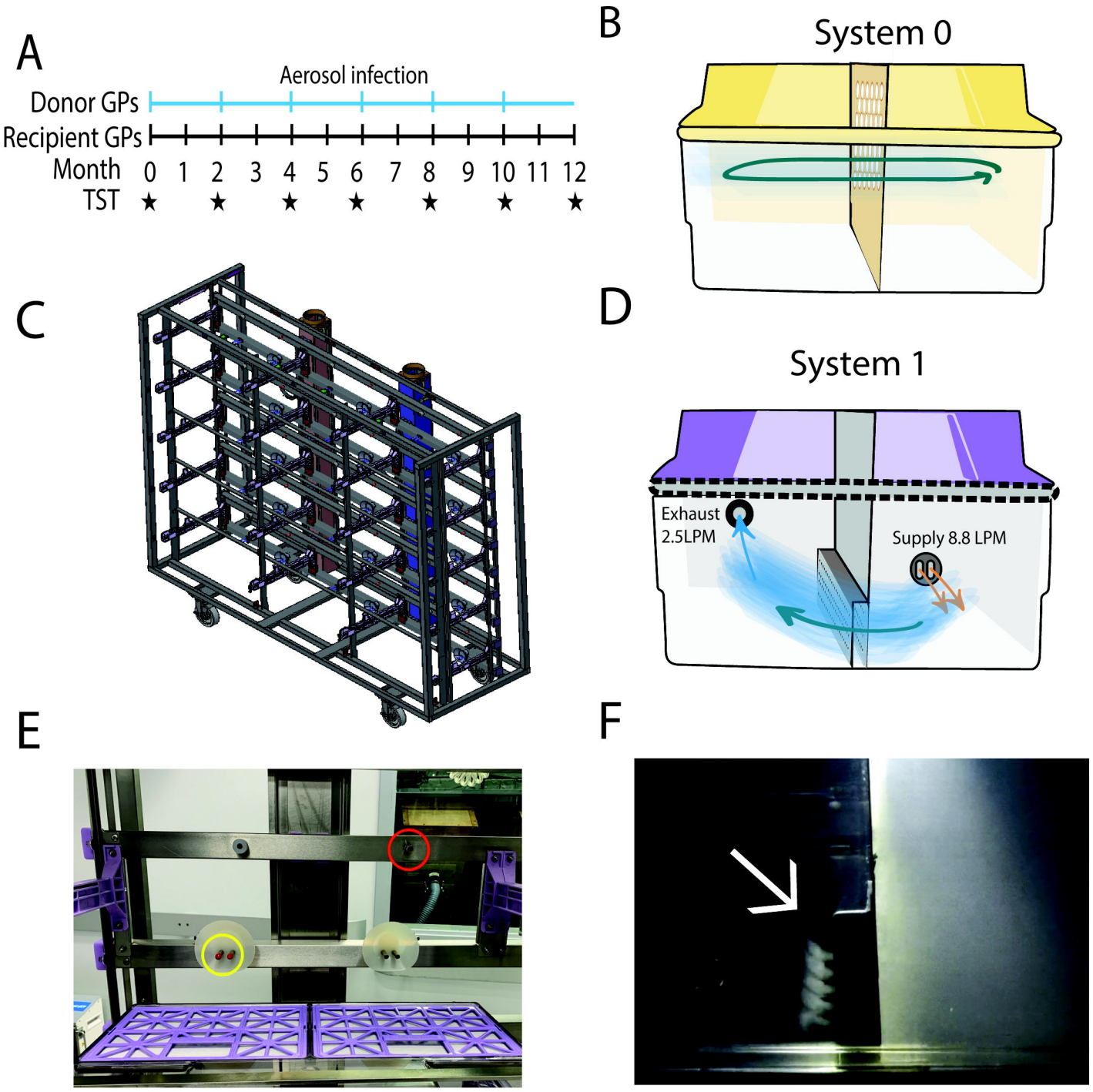
A
Aerosol infection
Donor GPs
Recipient GPs
Month 0 1 2 3 4 5 6 7 8 9 10 11 12
TST
B
System 0
C
D
System 1
Exhaust
2.5LPM
Supply 8.8 LPM
E
F

Figure 2

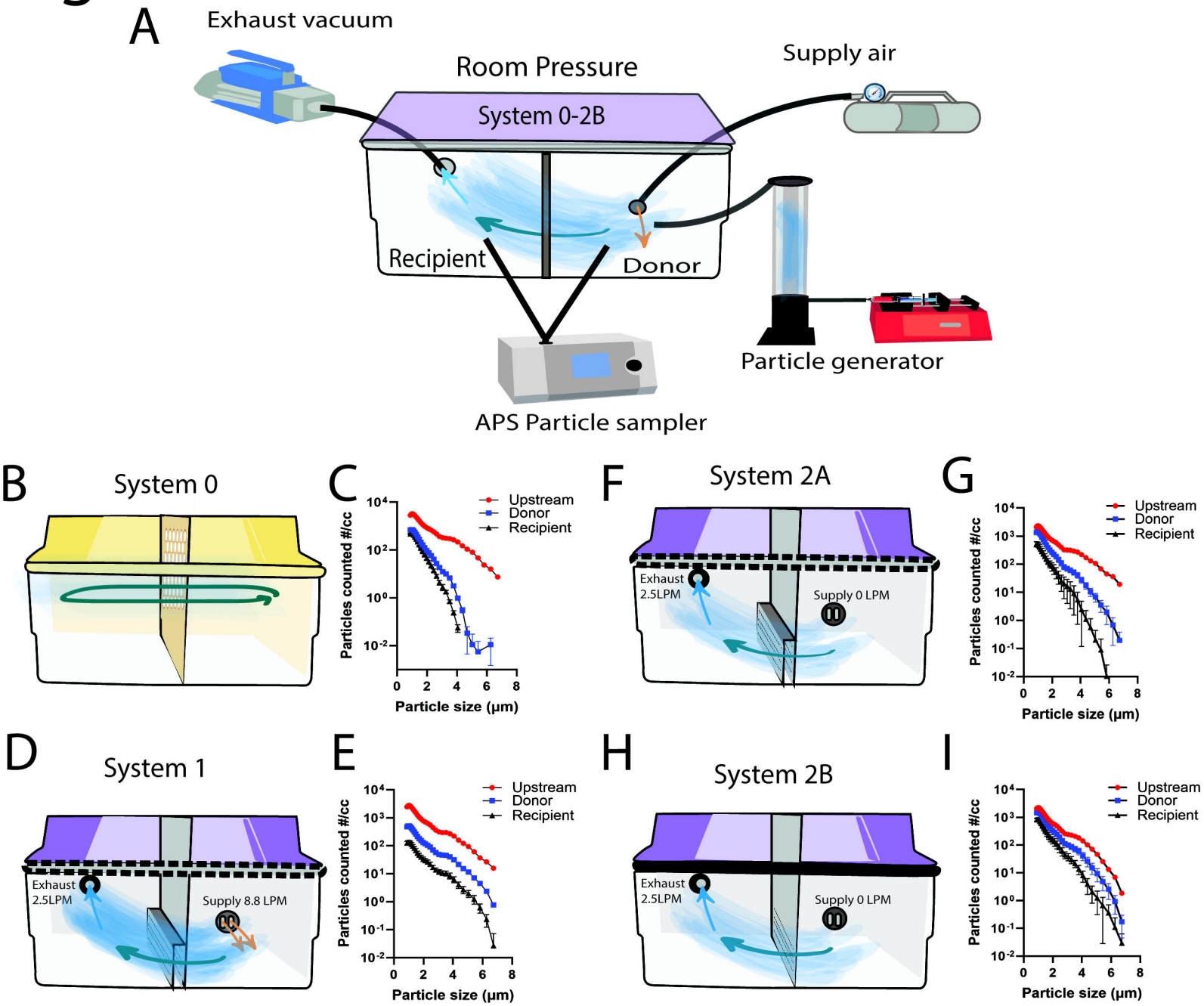
A
Exhaust vacuum
Room Pressure
Supply air
System 0-2B
Recipient
Donor
Particle generator
APS Particle sampler
B
System 0
C
Upstream
Donor
Recipient
Particles counted #/cc
Particle size (µm)
F
System 2A
Exhaust
2.5LPM
Supply 0 LPM
G
Upstream
Donor
Recipient
Particles counted #/cc
Particle size (µm)
D
System 1
Exhaust
2.5LPM
Supply 8.8 LPM
E
Upstream
Donor
Recipient
Particles counted #/cc
Particle size (µm)
H
System 2B
Exhaust
2.5LPM
Supply 0 LPM
I
Upstream
Donor
Recipient
Particles counted #/cc
Particle size (µm)

Figure 3

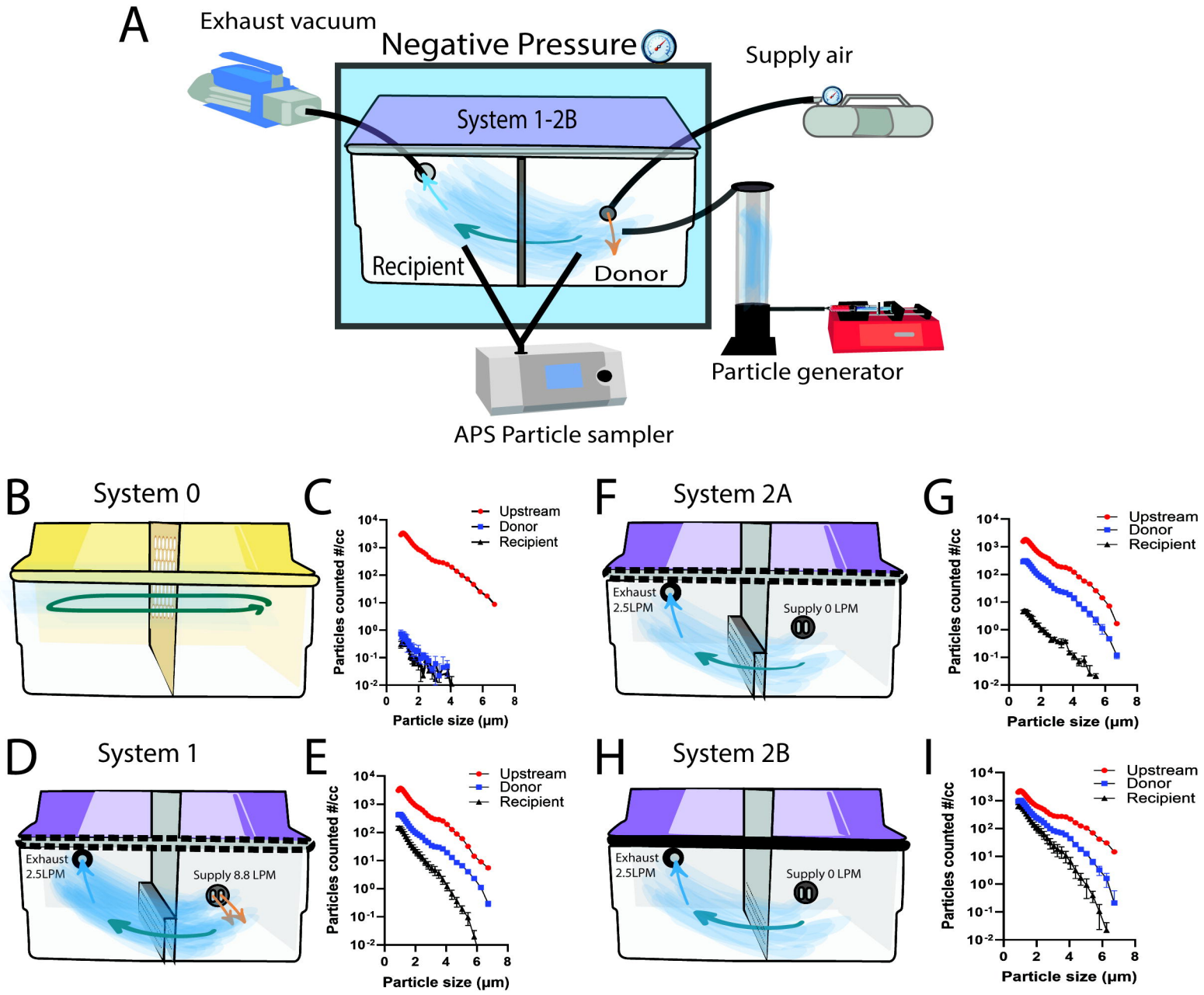
A
Exhaust vacuum
Negative Pressure
Supply air
System 1-2B
Recipient
Donor
Particle generator
APS Particle sampler
B
System 0
C
Upstream
Donor
Recipient
Particles counted #/cc
Particle size (µm)
F
System 2A
Exhaust
2.5LPM
Supply 0 LPM
G
Upstream
Donor
Recipient
Particles counted #/cc
Particle size (µm)
D
System 1
Exhaust
2.5LPM
Supply 8.8 LPM
E
Upstream
Donor
Recipient
Particles counted #/cc
Particle size (µm)
H
System 2B
Exhaust
2.5LPM
Supply 0 LPM
I
Upstream
Donor
Recipient
Particles counted #/cc
Particle size (µm)

Figure 4

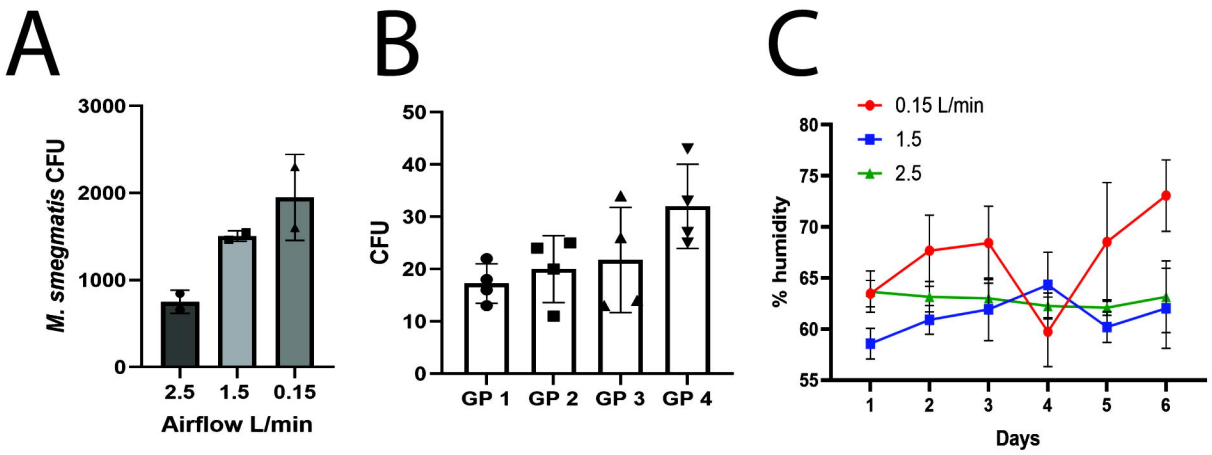
A
3000
2000
1000
0
M. smegmatis CFU
2.5
1.5
0.15
Airflow L/min
B
50
40
30
20
10
0
CFU
GP 1
GP 2
GP 3
GP 4
C
0.15 L/min
1.5
2.5
80
75
70
65
60
55
% humidity
1
2
3
4
5
6
Days

Figure 5

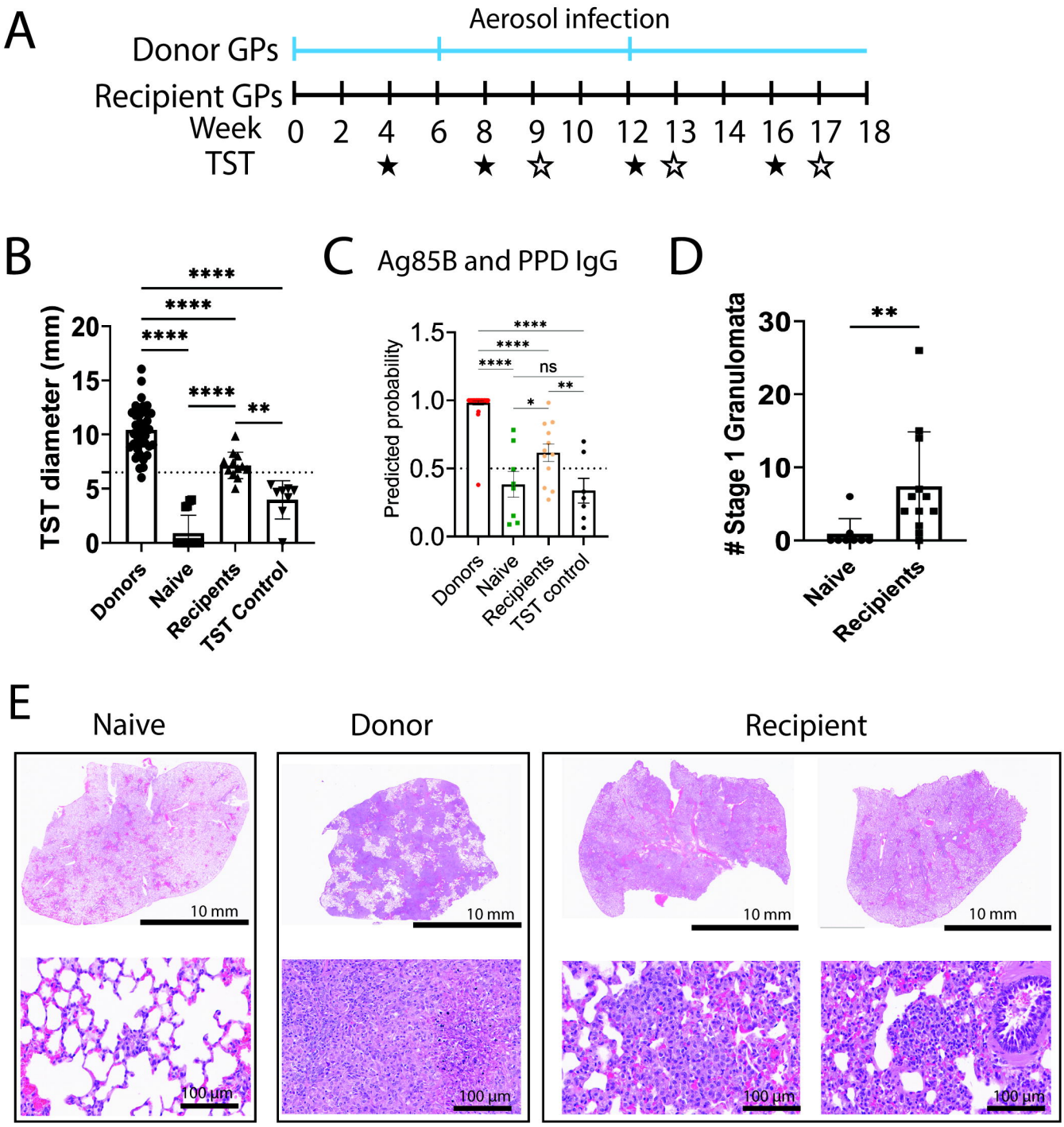
A
Aerosol infection
Donor GPs
Recipient GPs
Week 0 2 4 6 8 9 10 12 13 14 16 17 18
TST
B
TST diameter (mm)
Donors
Naive
Recipents
TST Control
C
Ag85B and PPD IgG
Predicted probability
ns
Donors
Naive
Recipients
TST control
D
Stage 1 Granulomata
Naive
Recipients
E
Naive
Donor
Recipient
10 mm
100 µm